Postprint of: Skarżyński Ł., Mechanical and radiation shielding properties of concrete reinforced with boron-basalt fibers using Digital Image Correlation and X-ray micro-computed tomography, Construction and Building Materials, Vol. 255 (2020), 119252, DOI: 10.1016/j.conbuildmat.2020.119252

Mechanical and radiation shielding properties of concrete reinforced with boron-basalt fibers using Digital Image Correlation and X-Ray micro-computed tomography

Łukasz Skarżyński

Faculty of Civil and Environmental Engineering, Gdańsk University of Technology, Poland
Email: lskarzyn@pg.edu.pl

Highlights

- Basalt fibers infused with boron oxide (BBF) can be successfully used as a concrete dispersed reinforcement.
- Radiation shielding properties of plain concrete and concrete reinforced with basalt fibers infused with boron oxide (BBF) are investigated.
- Mechanical and fracture properties of plain concrete and concrete reinforced with basalt fibers infused with boron oxide (BBF) are compared.
- Fracture process zone development using Digital Image Correlation is determined.
- Non-cracked and cracked material is analysed on the basis of 3D X-Ray micro-CT images.

Abstract

The paper presents experimental investigations of the radiation shielding, mechanical and fracture properties of concrete reinforced with 5 kg/m^3 of novel basalt fibers infused with boron oxide (BBF). However, further studies concerning other dosages i.e. 1 kg/m^3, 10 kg/m^3, 15 kg/m^3 and 20 kg/m^3 are currently carried out. Experiments with neutron source revealed that addition of BBF as a dispersed concrete reinforcement could improve the neutron radiation shielding of plain concrete by up to 25%. On the basis of mechanical tests, it turned out that compressive strength, tensile splitting strength and flexural of concrete reinforced with BBF were lower by up to 15% than analogous values for plain concrete. Simultaneously, shrinkage strain of BBF concrete was lower by about 10% than of plain concrete. Fracture process zone development on the surface of samples was investigated by Digital Image Correlation (DIC) using camera with the 36 megapixel matrix that allowed to obtain pixel size of 18 μm resulting in the length resolution equal approximately 60 pixel/mm whereas analyses of 3D material micro-structure, air voids, width and curvature of crack were carried out by X-ray micro-computed tomography (micro-CT) with 0.2 mm brass filter, voltage and the current equal 130 keV and 61 μA, respectively. The voxel size of the X-ray micro-CT was 39.68 microns. Experiments revealed that basalt fibers infused with boron oxide as a concrete dispersed reinforcement improved the ability of limiting micro-cracking area and bridging macro-cracking by up to 28%.

Keywords: air voids, boron-basalt fibers, concrete, crack, Digital Image Correlation, fracture zone, radiation shielding, X-ray micro-CT

1. Introduction

The application of concrete as a protective material in engineering structures intended for radioactive materials has been investigated for many years [1-12]. Structural concrete is designed not only to protect the population but also the external environment against the harmful effects of nuclear radiation. Nowadays, radioactive radiation is widespread which causes that shielding against it is a very important topic and is the subject of engineers' and scientists' research. A valuable shielding material in addition to increased protective ability should have the required strength as well as adequate durability. It is the fracture phenomenon that has a major impact on the durability of

concrete structures leading simultaneously to the reduction of material strength [13-15] thus, it is absolutely necessary to take an effort with aim to minimize cracking formation and evolution.

The idea of using basalt fibers infused with boron oxide additive as a dispersed concrete reinforcement in order to improve material radiation shielding properties and broaden the possibilities of application BBF concrete for protection against nuclear energy has been developed by Gulik and Biland [16]. Initial investigations of radiation shielding properties of concrete reinforced with BBF were presented in detail by Zorla et al. [17] where theory of process for producing the basalt-boron fibers was also described. The idea of basalt fibers infused with boron oxide (BBF) is based on the assumption that the protective properties of concrete will be improve while maintaining its mechanical properties with parallel improvement of material durability obtained due to limiting of micro-and macro-cracking. Uniform distribution of basalt fibers is their advantage over steel and polymers fibers. Nowadays, general research knowledge in the field radiation shielding properties of concrete reinforced with basalt fibers infused with boron oxide is quite limited [17-18]. Moreover, the phenomenon of fracture evolution in concrete reinforced with BBF is almost completely unrecognized.

The main goal of this manuscript is experimental research of radiation shielding properties as well as mechanical properties on the basis of compressive strength test, tensile splitting strength test, shrinkage test, tensile and residual strength in 3-point bending test. Besides, fracture phenomenon i.e. crack formation, evolution, shape and width in plain concrete and concrete reinforced with basalt fibers infused with boron oxide (BBF) was carefully investigated. At first, fracture process zone formation and evolution in terms of localized zone width, height and length, on the surface of samples, was measured and visualized by Digital Image Correlation (DIC) using NIKON D800 digital camera with the 36 megapixel matrix that allowed to obtain pixel size of 18 μm resulting in the length resolution equal approximately 60 pixel/mm. Digital Image Correlation (DIC) technique has already been efficiently used to experimentally analyze fracture phenomenon in a variety of materials [19-28]. Thereafter, 3D fracture phenomenon in terms of formation, evolution, width, shape and curvature of cracks was observed within a non-destructive X-ray micro-computed tomography (micro-CT) technique using SkyScan 1173 equipment. X-ray micro-computed technique is nowadays one of the most popular methods that gives the opportunities of effective analyses of material micro-structure as well as fracture phenomenon [29-41]. DIC and micro-CT tests delivered very useful quantitative information about fracture phenomenon in concrete reinforced with basalt fibers infused with boron oxide (BBF).

The main objective and novelty of this study are the investigations of the radiation shielding properties and mechanical properties of concrete reinforced with innovative basalt fibers infused with boron oxide (BBF) combined with the quantitative research of fracture phenomenon in terms of crack formation, evolution, shape and width using Digital Image Correlation (DIC) and X-ray micro computed tomography (micro-CT). The experimental research results allow to consider the boron-infused basalt fibers (BBF) as an interesting material for engineering applications.

2. Experimental procedure

The concrete mix consisted of cement CEM II/A-LL 42.5R, fly ash, aggregate and water. Aggregate was divided into three main fractions i.e. sand with maximum grain size equal 2 mm, gravel with the grain size in the range of 2 mm and 8 mm and gravel with the maximum grain size equal 16 mm (Figure 1). The sand point was equal to 41% and the water to cement ratio was established at w/c = 0.50. In order to properly design a concrete mix, the right proportions of coarse aggregate and sand should be selected so that they form a tight aggregate composition in concrete. The aggregate grain curve located in the area of good grain size (between boundary curves) guarantees proper workability and consistency of concrete mix with the lowest possible demand for cement paste

(cement and water) and minimal air content. It also provides low concrete permeability and less shrinkage.

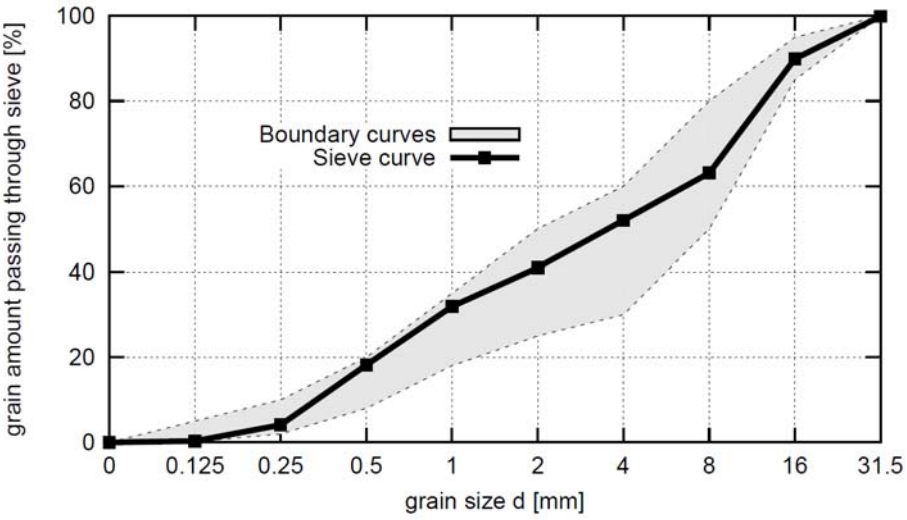

Figure 1: Distribution of aggregate particles

Additionally, fly ash was used as additive to concrete. It is widely used due to its high fineness (similar to cement), chemical and phase composition similar to clayey mineral raw materials and chemical activity, especially pozzolanic activity. Properly used fly ash has a positive effect on the properties of both fresh concrete mix and hardened concrete. It enables the production of high-quality, durable concrete in an economic and pro-ecological way. To improve the workability of fresh concrete mix, a small superplasticizer quantity was used. Thus, final mix is characterized by ratio including presence of water (w), cement (c), admixture (s) and addition (a) in a following way:

$$\frac{w+s}{c+(0.4\cdot a)}=0.46 \tag{1}$$

The used mix proportions are depicted in Table 1 and chemical composition of cement in Table 2.

Table 1: Concrete recipe details

Concrete components	**Concrete mix** (d_{50}=2 mm, d_{max}=16 mm)
Cement CEM II/A-LL 42.5R (c)	300 kg/m^3
Sand (0 - 2 mm)	735 kg/m^3
Gravel aggregate (2 - 8 mm)	430 kg/m^3
Gravel aggregate (8 - 16 mm)	665 kg/m^3
Fly ash (a)	70 kg/m^3
Superplasticizer (s)	1.8 kg/m^3
Water (w)	150 kg/m^3

Table 2: Chemical composition of cement in [%] (from the manufacturer)

SiO_2	Fe_2O_3	Al_2O_3	CaO	MgO	SO_3	Cl	Na_2O	K_2O	Others
21.68	3.39	4.38	64.79	1.17	2.91	0.083	0.26	0.49	0.85

In this study basalt fibers infused with boron oxide (BBF) were used. Basalt fibers had length equal 12 mm, diameter equal 13-17 microns (Figure 2), tensile strength not less than 1000 MPa and contained 12% of B_2O_3 enriched with 19.8% of ^{10}B and 80.2% of ^{11}B. This paper presents preliminary investigations of concrete reinforced with 5 kg/m^3 of BBF, however, further studies concerning other dosages i.e. 1 kg/m^3, 10 kg/m^3, 15 kg/m^3 and 20 kg/m^3 are currently carried out.

a)  b) 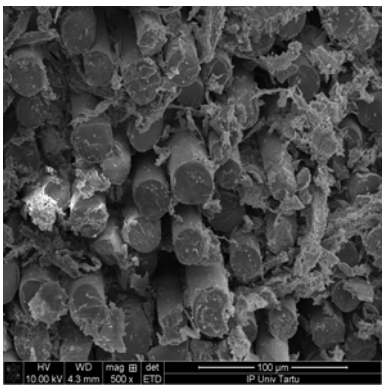 c) 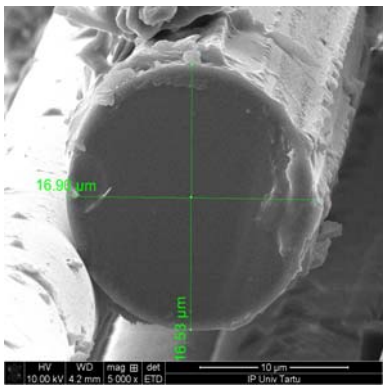

Figure 2: Boron-basalt fibers: a) macro view of fibers, b) enlarged 500 times view of fibers and c) enlarged 5000 times view of single fiber

Compressive strength, tensile splitting strength, flexural and residual strength in 3-point bending tests were carried out to compare BBF reinforced concrete and plain concrete properties. Compressive strength ($f_{c,cube}$) tests and tensile splitting strength (f_{ct}) tests were carried out on six cubes (150×150×150 mm) for each mixture. Flexural strength (f_{cf}) tests were carried out on 6 beams with the rectangular cross-section. The width and depth of beams were 150 mm, length was 600 mm and span length was 500 mm. Beams were mid-span notched with the height of 25 mm and width of 5 mm. Additionally, notch was used for mounting Crack Mouth Opening Displacement (CMOD) gauge. Compressive strength tests were carried out according to procedure described in EN 12390-3:2009 standard [42], splitting strength tests according to procedure described in EN 12390-6:2011 standard [43] and three-point bending tests according to procedure described in EN 14651:2005+A1:2007 standard [44]. All tests were performed after 28 days of curing according to procedure described in EN 12390-2:2009 standard [45]. On the basis of Polish recommendations [46] total shrinkage was investigated using Amsler apparatus and 3 beams with the dimension of 100×100×500 mm. Measurements of shrinkage were carried out for 112 days with the measurements made in 7, 14, 28, 56 day. Concrete total shrinkage that is one of the most common phenomenon during hardening of a fresh concrete mix. It leads to the irregular cracking of concrete that influences its strength and durability.

Additionally, to characterize fracture phenomenon, cubic specimens of plain concrete and concrete reinforced with basalt fiber infused with boron oxide (BBF) were subjected to variety of mechanical tests as: compression strength, splitting strength and wedge splitting (WST). Dimensions of the cubic samples i.e. 70×70×70 mm have been properly selected in order to be totally visible in the flat panel of the X-ray micro-CT system. Initially, fracture process zone formation and evolution, on the

surface of samples, was measured and visualized by Digital Image Correlation (DIC) but only during the wedge splitting tests (WST). Cubic samples intended for WST test were initially notched with the height of 15 mm and width of 5 mm. Samples were supported on the linear, square steel bar and tested with a controlled displacement rate of 0.002 mm/min. To measure fracture development where Crack Mouth Opening Displacement (CMOD) gauge was situated in the notch. Digital Image Correlation procedure was carried out using NIKON D800 digital camera with the 36 megapixel matrix that allowed to obtain pixel size of 18 μm resulting in the length resolution equal approximately 60 pixel/mm. Camera was placed in front of the tested specimen which surface was covered with the yellow-black speckle pattern. The digital images were taken every 6 seconds during test. Inspection window was assumed to be a square with the dimension of 120 pixels. It was twice greater than the biggest speckle i.e. ≥ 60 pixels. DIC scanning resolution was assumed to be 5 pixels [47-48]. Testing station used for DIC experiments is presented in Figure 3.

Figure 3: View on the DIC testing station. Digital NIKON D800 camera is mounted on a tripod perpendicularly to the concrete cubic sample during Wedge Splitting Test (WST) carried out using Instron 5569 static machine

To characterize and visualize 3D fracture zone during compression, splitting and wedge splitting test (WST) X-ray micro-CT SkyScan 1173 scanner with 0.2 mm brass filter was used. The X-ray source voltage and the current were equal 130 keV and 61 μA, respectively. The voxel size of the X-ray micro-CT was 39.68 microns whereas the shutter speed equaled 4000 ms. The sample was scanned at 180 degrees with a single rotation step of 0.2 degrees. Since the basalt fibers have approximately the same density as basic components of concrete and have diameter equal 13-17 microns (about 3 times smaller than image resolution) it was technically not possible to distinguish them from concrete. To distinguish air voids, the threshold value in the range of 0-60 was established. Experimental procedure started from initial micro-CT scan of non-cracked sample in order to gather all necessary information, concerning initial porosity and material microstructure. Compressive strength test was carried out according to procedure described in EN 12390-3:2009 standard [42] (instead of smaller samples tested), however, it was stopped just before specimen failure in order to enable micro-CT scanning. Splitting strength test was carried out according to procedure described in EN 12390-6:2011 standard [43] (instead of smaller samples tested). After the sample failure it was sealed with the adhesive tape in order to enable micro-CT scanning of entire sample. Wedge Splitting Tests (WST) were carried out on notched cubic samples identical to those used in DIC research. Testing station used for micro-CT experiments is presented in Figure 4.

Moreover, in order to verify air content obtained by air pressure method, describe and visualize air distribution in plain concrete and concrete reinforced with BBF micro-CT test were performed [49-50].

Dimensions of the tested samples were presented in Figure 5.

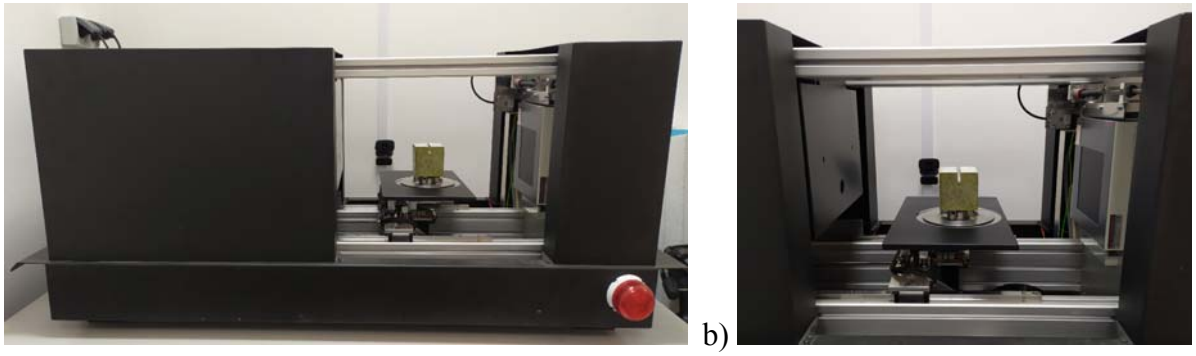

Figure 4: Micro-CT 1173 Skyscan X-ray micro-tomograph testing station: a) general view and b) zoom on the sample after Wedge Splitting Test mounted on the rotation table

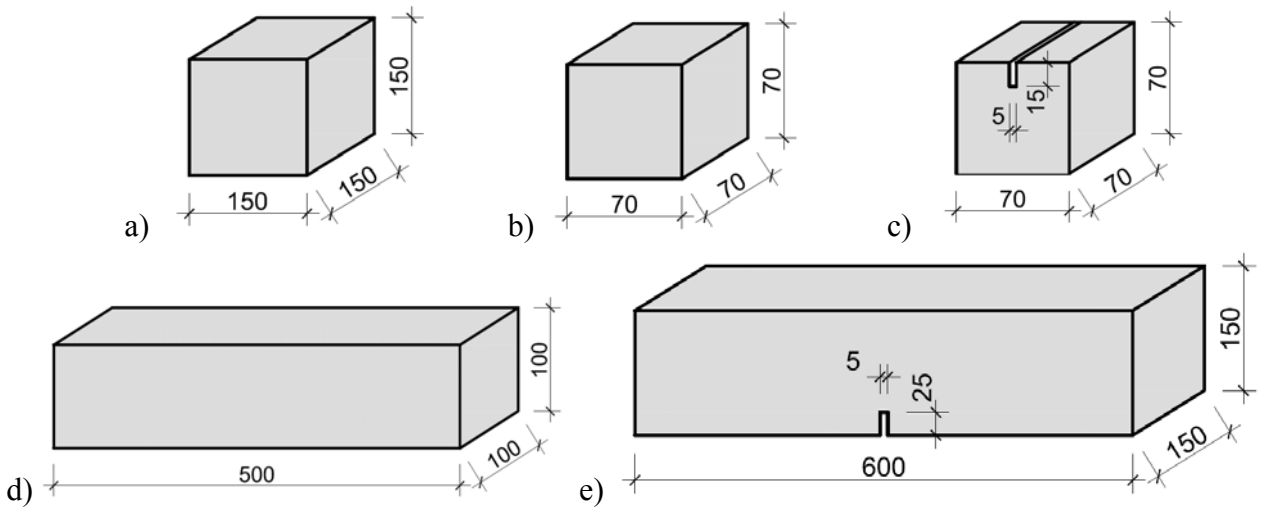

Figure 5: Dimensions of the tested samples: a) cubes for mechanical compressive and splitting tests, b) cubes for micro-CT compressive and splitting tests, c) cubes for DIC and micro-CT wedge splitting tests (WST), d) beams for shrinkage tests and e) beams for 3-point bending tests

3. Distribution of macro-voids

Before sample preparation, tests on fresh plain concrete and concrete with addition of basalt fibers infused with boron oxide (BBF) were carried out. The fresh concrete properties were determined based on Vebe slump test, Vebe time test and air content pressure test (Table 3). Vebe slump and Vebe time are quite simple and popular tests to determine consistency of fresh concrete mix. Increase of the Vebe time usually results in decreasing of concrete workability. Both mixes revealed similar workability, however, workability of concrete reinforced with basalt-boron fibers (BBF) was a bit worse. Air content is a very important property of fresh concrete mix. It can influence final properties of hardened concrete such as workability, strength and durability. It is still unclear whether the addition of fibers increases [51-53] or decreases [54] the content of air pores in concrete. In experiments, air content in fresh plain concrete (3.4%) was higher by about 0.6% than in fresh concrete reinforced with BBF (2.8%) that is in agreement with research work by [45]. Procedure of

air pressure method, concerning the way of filling the tube and time of vibration, was, obviously, the same. Density of fresh concrete reinforced with BBF was smaller by about 1.5% than of fresh plain concrete. Temperature of both concrete mixes was similar.

Table 3: Properties of fresh concrete mix

Concrete mix	Temperature [^{0}C]	Vebe slump test [mm]	Vebe time [s]	Air content [%]	Density [kg/m^3]
Concrete	14.9	140	3.8	3.4	2343.0
Concrete with 5 kg/m^3 BBF	14.2	125	4.1	2.8	2312.0

Figures 6 and 7 and Table 4 show the initial 3D air void content and air void distribution in non-cracked concrete and BBF concrete specimens measured by micro-CT. The air pores were analysed in relation to open and closed porosity. The pores than intersect the boundaries of volume of interest (VOI) are defined as open pores. On the contrary, pores that are entirely located inside VOI are treated as closed ones. Air volume in non-cracked plain concrete specimen varied from 5785.61 mm^3 to 7196.16 mm^3 which equals 2.42% and 3.01% of total air volume, respectively. Pores with diameter smaller than 0.5 mm, in the range of 0.51 mm – 1.50 mm and larger than 1.51 mm represented approximately 15%, 40% and 45% of total porosity, respectively. Measured closed porosity varied between 1.88% and 2.28% whereas open porosity varied between 0.54% and 0.73%. Air volume in non-cracked BBF reinforced concrete specimen varied from 7918.72 mm^3 to 9492.63 mm^3 which equals 3.22% and 3.85% of total air volume, respectively. Pores with diameter smaller than 0.5 mm, in the range of 0.51 mm – 1.50 mm and larger than 1.51 mm represented approximately 15-20%, 35% and 45-50% of total porosity, respectively. Measured closed porosity varied between 2.34% and 2.99% whereas open porosity varied between 0.75% and 0.88%. Total porosity obtained by 3D X-ray micro-CT analyses in concrete reinforced with BBF was higher by about 30% than in plain concrete that is in agreement with research works [51-53]. Total porosity was smaller by about 10-30% than porosity obtained in the air pressure method in case of plain concrete and higher by about 15-40% in case of concrete reinforced with BBF. Obtained results clearly show that air pressure method may not be accurate. This is particularly important because air pressure method is the most popular method of assessing fresh concrete mix for its future frost resistance. More reliable could be AVA (Air Void Analysis) technology that allows to assess spacing factor, specific surface area, and total air content.

Table 4: Air void analysis in non-cracked specimens by micro-CT

Specimen number	Diameter distribution of pores [%] within total porosity			Volume of pores [mm^3]	Volume of pores [%] within entire sample volume	Volume of closed pores [%] within entire sample volume	Volume of open pores [%] within entire sample volume
	≤0.50 mm	0.51-1.50 mm	≥1.51 mm				
Concrete "1"	15.21	38.89	45.90	6694.10	2.80	2.13	0.67
Concrete "2"	12.55	40.12	47.33	5785.61	2.42	1.88	0.54
Concrete "3"	16.34	42.87	40.79	7196.16	3.01	2.28	0.73
BBF "1"	18.25	32.52	49.23	9492.63	3.86	2.99	0.87
BBF "2"	17.36	35.89	46.75	7918.72	3.22	2.34	0.88
BBF "3"	16.98	34.87	48.15	8238.42	3.35	2.60	0.75

a) 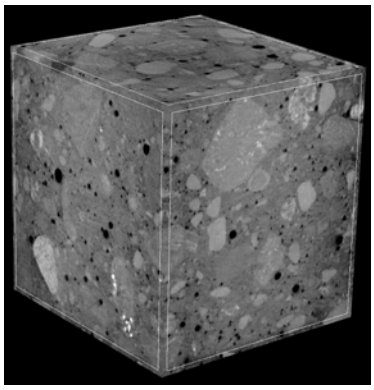 b) 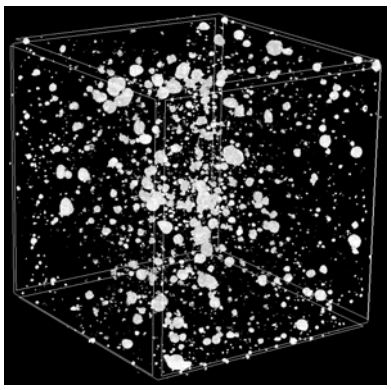 c) 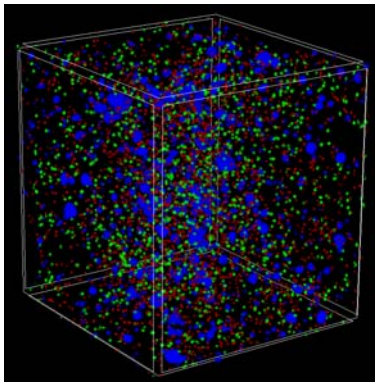

Figure 6: Non-cracked plain concrete cubic specimen (Concrete "1" from Table 4) images by 3D micro-CT: a) general view, b) distribution of pores and c) diameter distribution of pores ≤ 0.50 mm (red colour), in range 0.51 mm – 1.50 mm (green colour) and ≥ 1.51 mm (blue colour)

a) 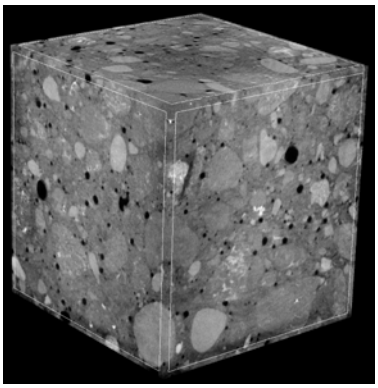 b) 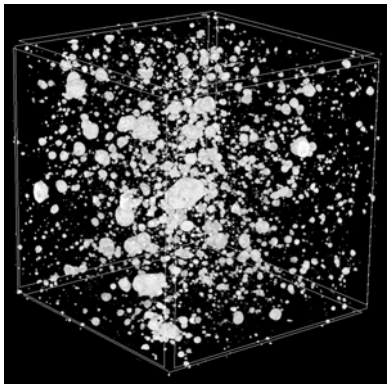 c) 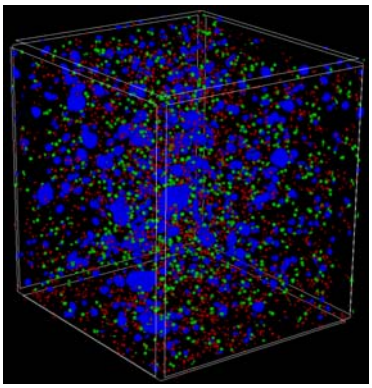

Figure 7: Non-cracked BBF concrete cubic specimen (BBF "1" from Table 4) images by 3D micro-CT: a) general view, b) distribution of pores and c) diameter distribution of pores ≤ 0.50 mm (red colour), in range 0.51 mm – 1.50 mm (green colour) and ≥ 1.51 mm (blue colour)

To analyse changes in porosity within sample height and width, total volume of sample was divided into 5 mm thick vertical and horizontal sub-volumes within which air volume was measured. Distribution of air pores in non-cracked concrete cubic specimen (Concrete "1" from Table 4) and BBF concrete cubic specimen (BBF "1" from Table 4) is compared in Figure 8.

a) 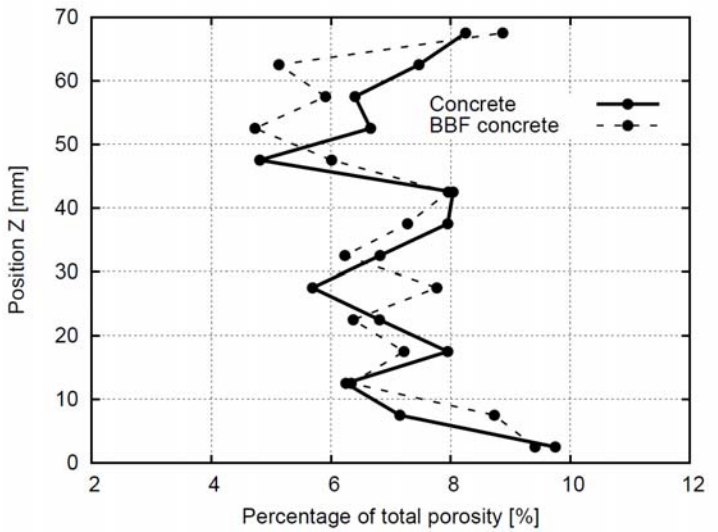

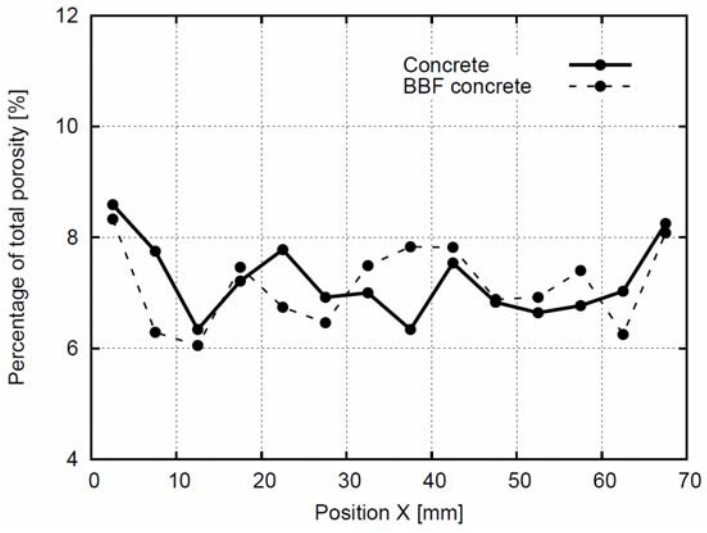

b)

Figure 8: Distribution of porosity in concrete (Concrete "1" from Table 4) and BBF concrete (BBF "1" from Table 4) along: a) sample height and b) sample width

The distribution of porosity is very similar and quite uniform along width and height for both concrete and BBF reinforced sample. However, a slight increase in porosity can be observed at the border surfaces of the samples which may be caused by the different vibration conditions in the neighbourhood of the mold walls during concreting.

3. Radiation shielding properties

Basalt fibers with improved radiation shielding properties, due to addition of boron oxide, are believed to extend the application possibilities of concrete for nuclear material management. Within this work, experiments with Pu-Be neutron source and neutron detector were conducted in Chernobyl on plain concrete and concrete with addition of 5 kg/m^3 of basalt fibers infused with 12% of B_2O_3 enriched with 19.8% of ^{10}B and 80.2% of ^{11}B cubes with dimension of 100×100×100 mm to investigate the neutron attenuation. Thickness of concrete reinforced with basalt fibers infused with boron oxide (BBF) varied from 100 mm to 500 mm.

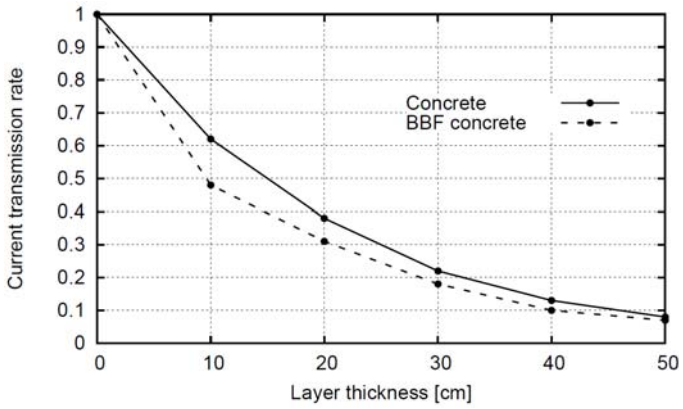

Figure 9: Variation of the neutron spectrum transmission with various thickness of concrete

Experiments with Pu-Be neutron source and neutron detector proved that concrete reinforcement in terms of basalt fibers infused with boron oxide may lead to the improvement of the neutron radiation shielding for fast neutron spectrum. Increase in neutron radiation shielding properties varied from 10% for layer thickness equal 50 cm to 25% for layer thickness equal 10 cm (Figure 9). Thus,

application of BBF as the concrete reinforcement is promising in terms of reduction of the concrete thickness in structures intended for nuclear material management.

4. Mechanical properties of concrete and BBF concrete

4.1. Compressive strength

The specimens reinforced with basalt fiber infused with boron oxide (BBF) exhibited a reduction in the compressive strength $f_{c,BBF}$ compared to the reference plain concrete f_c. Mean compressive strength of plain concrete (f_c = 47.60 MPa) was higher by about 15% than mean strength of concrete reinforced with BBF fibers ($f_{c,BBF}$ = 41.29 MPa) with similar standard deviation values. Similarly, the tensile splitting strength of concrete reinforced with BBF was decreased in comparison to plain concrete (Table 5).

Table 5: Mechanical properties of hardened concrete and concrete reinforced with BBF

Mechanical test type	Material	Type of sample	Number of samples	Average density [kg/m^3]	Standard deviation [kg/m^3]	Average stress [MPa]	Standard deviation [MPa]
Compressive strength	Concrete	Cube 150×150×150 mm	6	2359.2	15.26	47.60	1.66
	BBF concrete		6	2328.3	17.74	41.29	1.30
Tensile strength	Concrete	Cube 150×150×150 mm	6	2361.1	6.99	3.46	0.19
	BBF concrete		6	2325.0	25.41	3.01	0.36
Flexural strength	Concrete	Beam 150×150×600 mm	6	-	-	3.60	0.20
	BBF concrete		6	-	-	3.20	0.18

4.2. Tensile and flexural strength

Mean splitting strength of plain concrete (f_{ct} = 3.45 MPa with standard deviation 0.19 MPa) was higher by about 15% than mean strength of concrete reinforced with BBF fibers ($f_{ct,BBF}$ = 3.01 MPa with standard deviation 0.36 MPa) (Table 5). Average flexural strength of plain concrete ($f_{cf,}$ = 3.60 MPa with standard deviation 0.20 MPa) was higher by about 12.5% than the average flexural strength ($f_{cf,BBF}$ = 3.20 MPa with standard deviation 0.18 MPa) for concrete reinforced with BBF. Basalt fibers, like other fiber types, have a tendency to decrease workability of fresh concrete that generates higher effort during compaction and sometimes there is a risk of reduction of the concrete strength. In addition, total porosity in BBF concrete, obtained by micro-CT, is higher by about 30% than in plain concrete that also leads to the reduction of material strength. However, it is worth to mention that the ratio of the tensile strength to the compression strength i.e. f_{ct} / f_c, $f_{cf,}$ / f_c and $f_{ct,BBF}$ / $f_{c,BBF}$, $f_{cf,BBF}$ / $f_{c,BBF}$ is always similar and equal 0.072 – 0.077.

The tensile behaviour of BBF concrete was additionally evaluated in terms of residual flexural tensile strength values determined from the load-CMOD curve. The residual flexural tensile strength was calculated for $CMOD_1$ = 0.15 mm, $CMOD_2$ = 0.25 mm and $CMOD_3$ = 0.35 mm. Figure 10 presents the experimental F – CMOD curves whereas Table 6 shows the experimental results. The average residual flexural strength of plain concrete was equal $f_{R,0.15}$ = 2.24 MPa, $f_{R,0.25}$ = 1.15 MPa and $f_{R,0.25}$ = 0.59 MPa and was greater by about 15% than the average residual tensile strength of concrete reinforced with BBF ($f_{R,0.15}$ = 2.06 MPa, $f_{R,0.25}$ = 0.99 MPa and $f_{R,0.35}$ = 0.52 MPa).

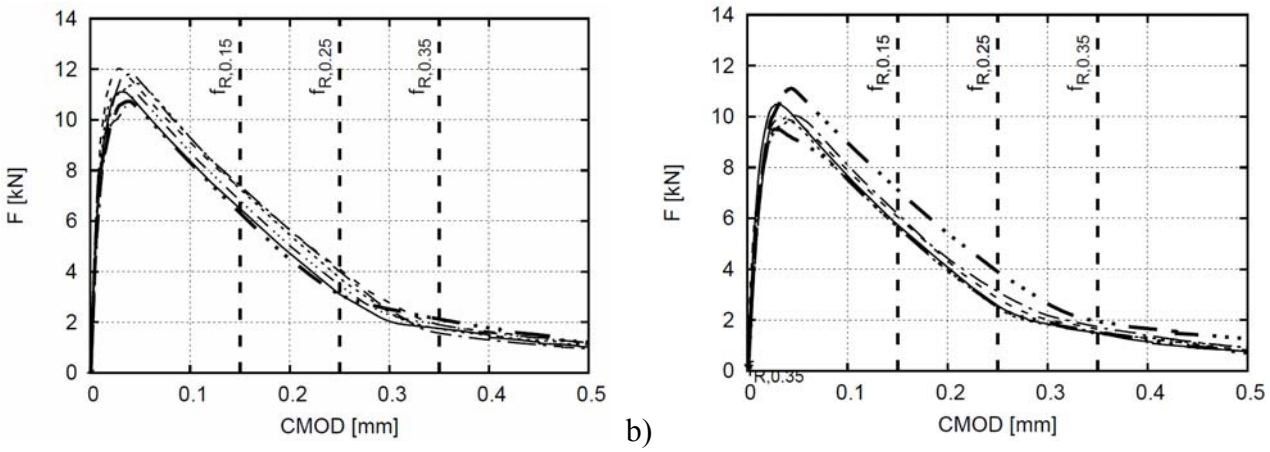

Figure 10: Experimental *F*-CMOD curves for 6 beams during flexural test: a) plain concrete and b) concrete reinforced with BBF

Table 6: Residual flexural strength of plain concrete and BBF reinforced concrete

Mechanical test type	Material	Average $f_{R,0.15}$ [MPa]	Standard deviation [MPa]	Average $f_{R,0.25}$ [MPa]	Standard deviation [MPa]	Average $f_{R,0.35}$ [MPa]	Standard deviation [MPa]
Three point bending	Concrete	2.24	0.14	1.15	0.14	0.59	0.06
	BBF concrete	2.06	0.27	0.99	0.17	0.52	0.06

4.3. Concrete shrinkage

Final total shrinkage strain for plain concrete was equal 1.65‰ whereas for concrete reinforced with BBF fibers was equal 1.52‰ (Figure 11). Increase of total shrinkage shown similar tendency since the majority (80% of final shrinkage strain) of strain increase was observed within 14 days. After that, gentle growth of total shrinkage strain was observed for both mixes. Nevertheless, similar evolution of total shrinkage strain curve and quite high final shrinkage strain leads to the conclusion that both type of concrete mixes require careful curing early during stages of hardening in order to minimize shrinkage cracking.

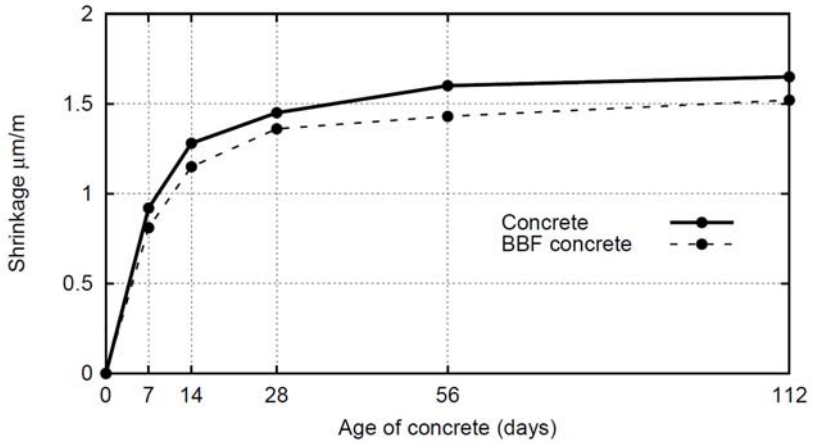

Figure 11: Evolution of total shrinkage with age of concrete: (a) plain concrete and (b) BBF reinforced concrete

5. Characterization of the fracture process by Digital Image Correlation

Figure 12 presents vertical force F versus CMOD curves obtained during WST tests for both plain concrete and concrete reinforced with basalt fiber infused with boron oxide (BBF). Force-CMOD diagrams revealed that stiffness of plain concrete and BBF reinforced concrete is similar in the elastic regime whereas difference in ductility was observed in post-peak regime. This phenomenon is explainable by the presence of fibers and non-uniform distribution of aggregate particles. The maximum force in plain concrete was equal 3.83 kN and was by about 10% higher than maximum force registered for BBF reinforced concrete which was equal 3.50 kN. Residual vertical forces in BBF reinforced concrete were $F_{res,0.15}$=1.81 kN (at CMOD=0.15 mm) and $F_{res,0.25}$=0.72 kN (at CMOD=0.25 mm) whereas residual vertical forces in plain concrete were $F_{res,0.15}$=1.48 kN and $F_{res,2.5}$=0.38 kN, respectively. Residual force values of BBF concrete were higher by about 20% and 90% than corresponding values of plain concrete. It means that BBF concrete characterizes with greater ductility due to presence of fibers that have the ability of bridging micro-cracks.

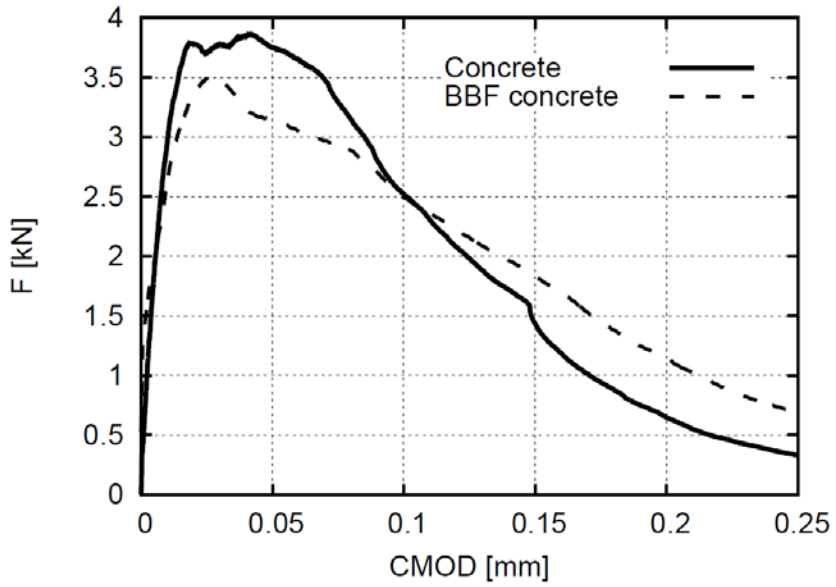

Figure 12: Force - CMOD curves of Wedge Splitting Test (WST): (a) plain concrete, (b) concrete reinforced with basalt fiber infused with boron oxide (BBF)

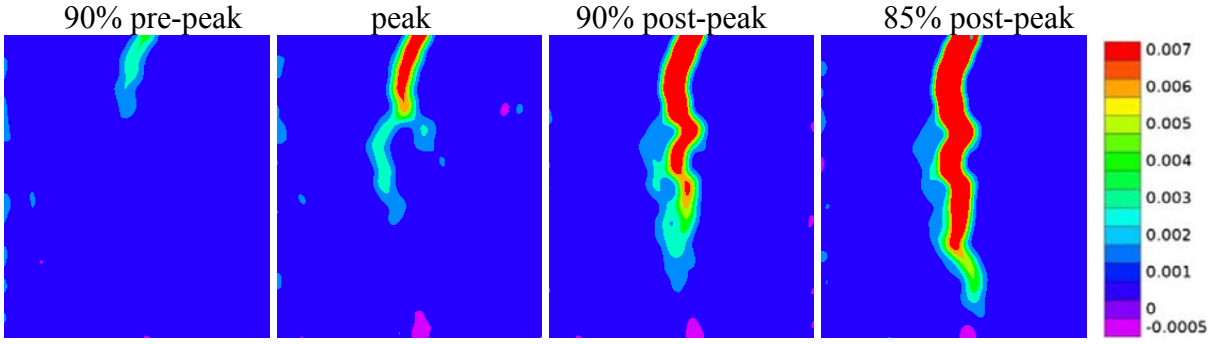

(a)

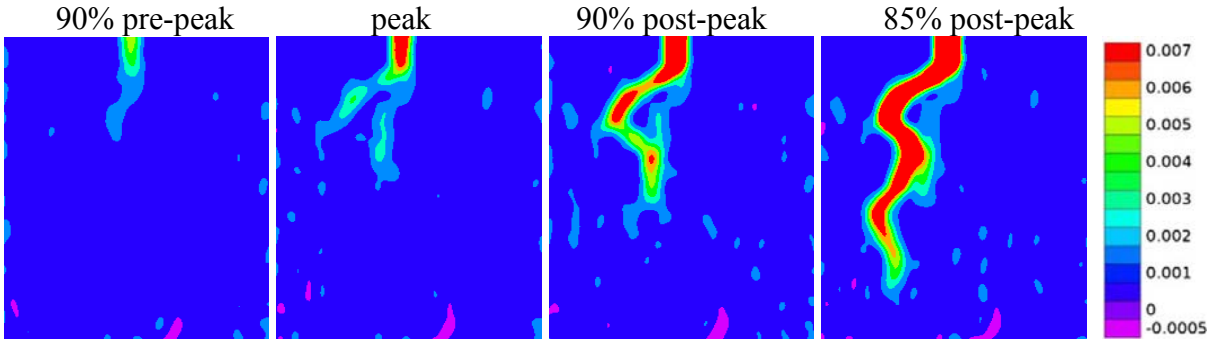

(b)

Figure 13: Evolution of fracture below the notch, visualized by DIC technique, during WST test: (a) plain concrete, (b) BBF reinforced concrete

A fracture zone was initially observed at 90% of the peak load value on the force-CMOD curve. After formation, fracture zone evolved by propagating between aggregate grains and micro fibers whereby its shape was strongly curved (Figure 13). Both concrete mixes were characterized by the similar horizontal normal strain profiles with the maximum value equal about 0.07% and similar horizontal displacement profiles with the value equal about 0.11 mm (Figure 14). Macro-crack could have been observed in the post-peak regime at 85% of the maximum vertical load.

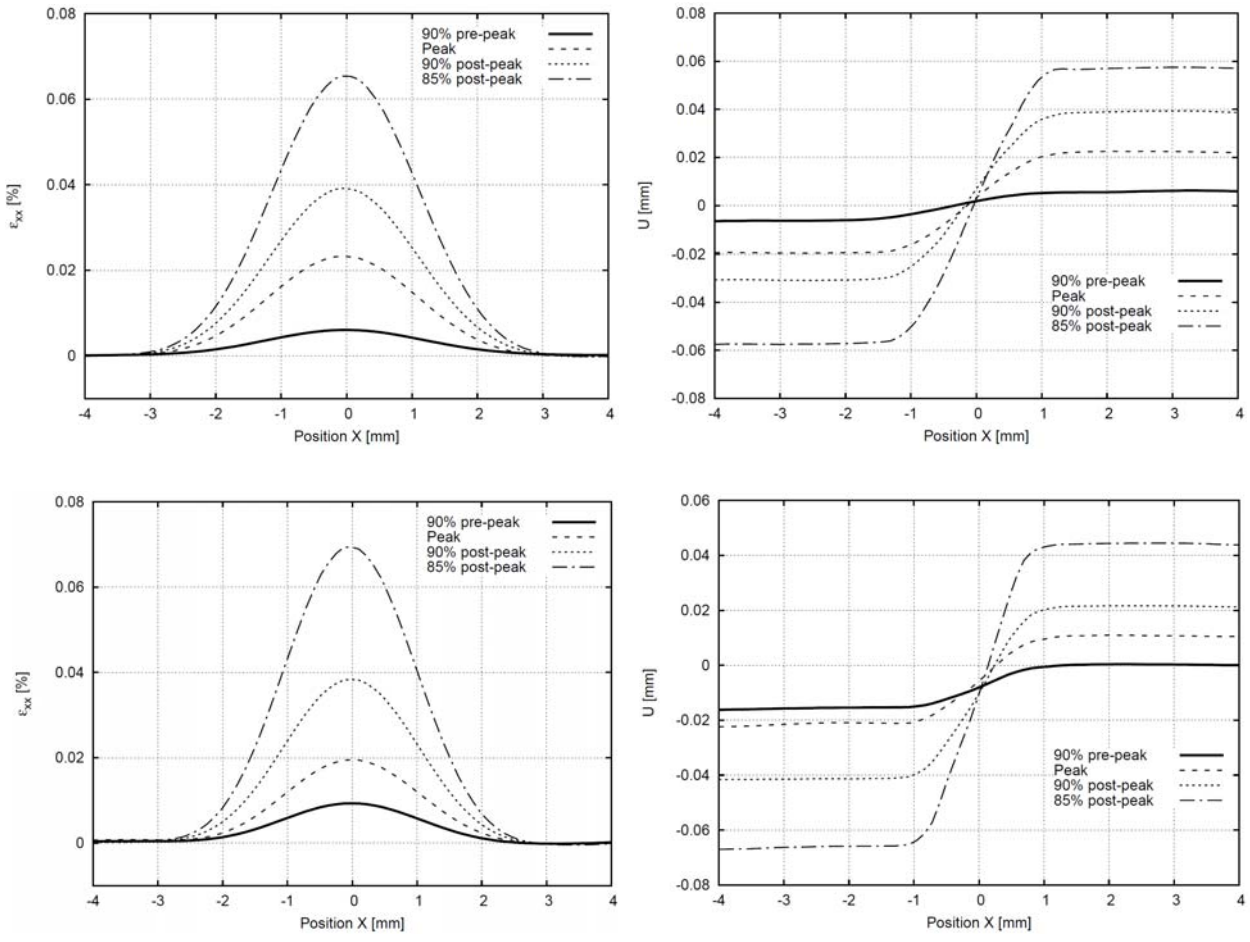

(A)

(B)

Figure 14: Horizontal normal strain ε_{xx} profiles (left column) and horizontal displacement U profiles (right column) measured by DIC technique along the horizontal cross-section just below the notch for (a) 85% pre-peak (fracture zone formation), (b) 90% pre-peak, (c) peak and (d) 85% post-peak (macro-crack formation): (A) plain concrete, (B) BBF reinforced concrete (Position X is the length in [mm] of the analyzed cross-section where 0 is the middle of the notch)

The measurement of the fracture zone width based on the approximation of strain profiles with the normal Gauss distribution and calculations of standard deviation σ [26]. The width, length and height of the fracture zone measured just before the macro-crack formation, were equal w_{fz}=4.71 mm, l_{fz}=47.39 mm, h_{fz}=45.37 mm in plain concrete (Figures 14Ad and 13a) and $w_{fz,BBF}$=4.15 mm, $l_{fz,BBF}$=52.75 mm, $h_{fz,BBF}$=42.72 mm in concrete reinforced basalt fiber infused with boron oxide (Figures 14Bd and 13b). The measured width of the fracture zone in plain concrete was about 15% larger than in BBF concrete. It means that basalt fibers infused with boron oxide have the ability of limiting micro-cracking area. Additionally, the fracture zone of the BBF concrete is longer by about 10% than in plain concrete which leads to the more ductile response in the softening regime.

6. Characterization of the fracture process by micro-CT

Mechanism of failure during compression was similar for plain concrete and concrete reinforced basalt fiber infused with boron, however, wider cracks in plain concrete, up to w_c=2.26 mm, than in BBF concrete, up to $w_{c,BBF}$=1.47, might have been observed (Figure 15). Final cracking appeared as a connected matrix with the main vertical cracks that evolved through the entire height of the samples and proved to be decisive. Nevertheless, diagonal cracks were noticed as well. Presence of randomly distributed aggregate particles and micro BBF fibers resulted in curvature of cracks. Generally speaking, cracking initially formed in the nearest neighbourhood of the aggregate particles where so called Interfacial Transition Zones (ITZs) occur that are considered to be the weakest zones in hardened concrete [55-56]. Next, cracks connected through a bridging mechanism by propagating mainly within cement matrix.

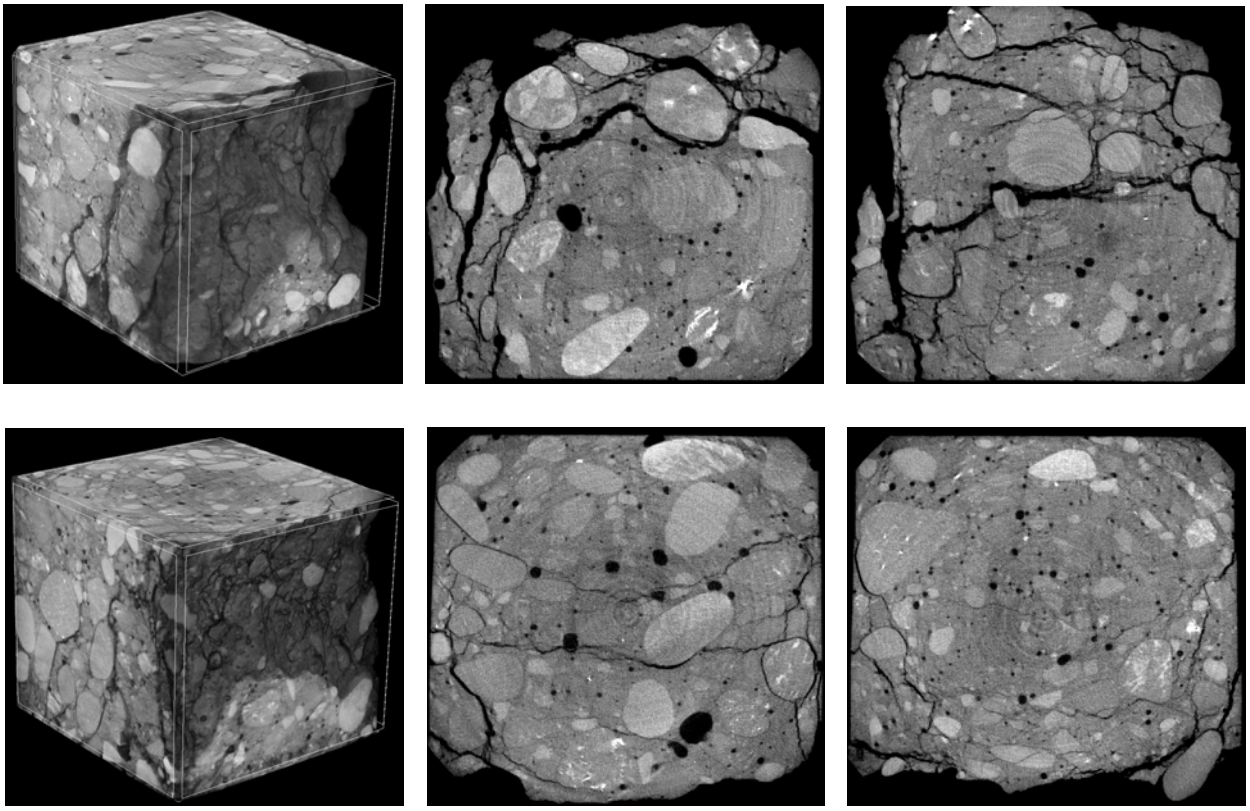

Figure 15: X-ray micro-CT images of cracked cubic specimens close to failure during uniaxial compression test: (A) plain concrete and (B) BBF reinforced concrete where (a) 3D view of entire sample, (b) and (c) horizontal cross-sections

Mechanism of failure during splitting was also similar for plain concrete and concrete reinforced basalt fiber infused with boron. The main attention in this test was focused on surface of the cracked area. It is clearly visible that cracked area was non-uniform and strongly curved along sample depth and height (Figures 16Ab and Bb). The surface of cracked area in concrete reinforced with basalt fiber infused with boron oxide in plain concrete was equal $A_{c,BFF}$=15766.58 mm^2 and was by about 9% higher than the surface of crack area in plain concrete equal A_c=14418.83 mm^2. It means that cracked area in BBF concrete is more curved than in plain concrete that may lead to the conclusion that evolution of the crack in BBF concrete is more sophisticated (crack is propagating between aggregate particles and micro BBF fibers) than in plain concrete, thus, a more ductile response in a post-peak regime can be obtained.

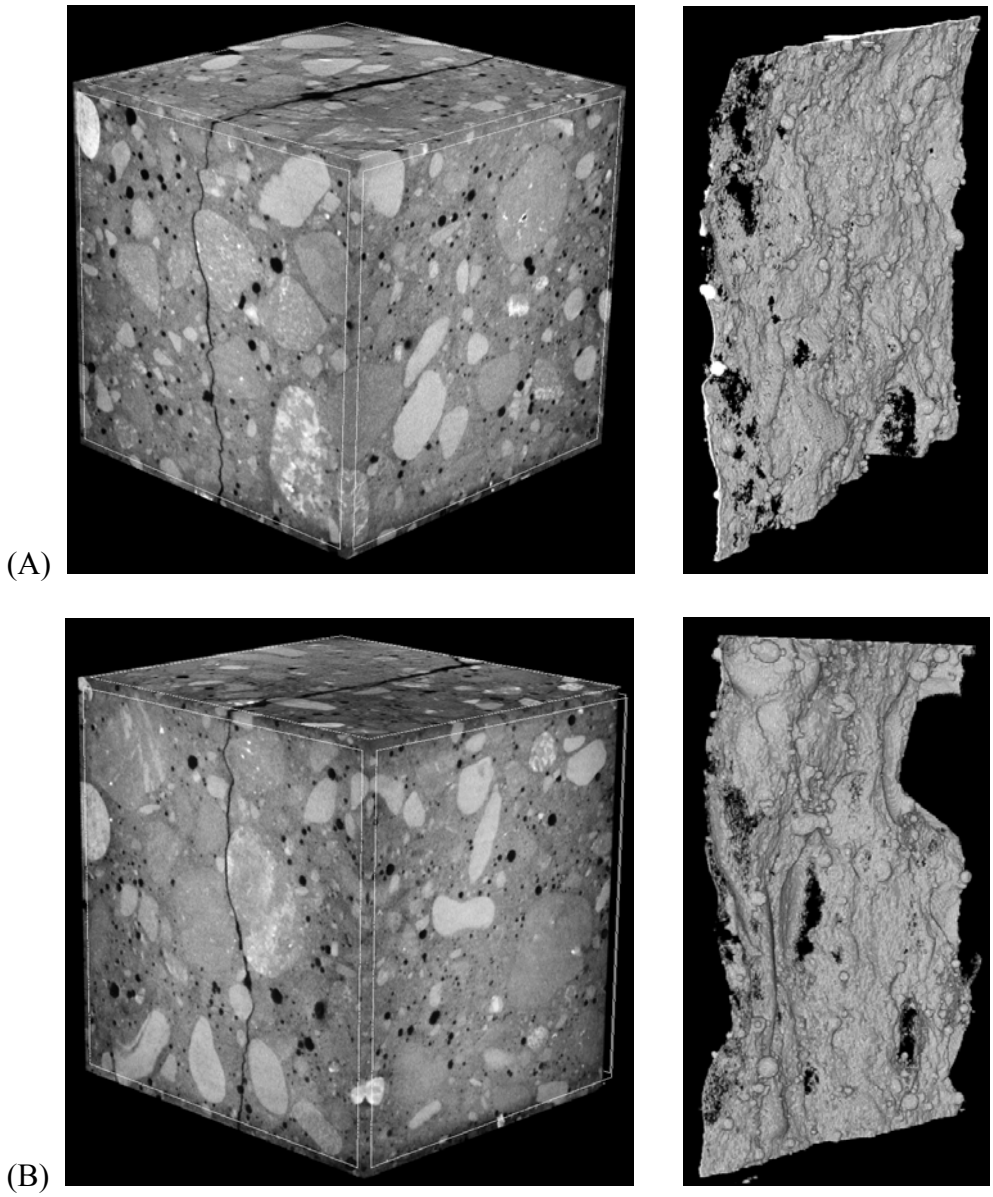

Figure 16: X-ray micro-CT images of cracked cubic specimens during splitting test: (A) plain concrete and (B) BBF reinforced concrete where (a) 3D view of the entire sample and (b) 3D view of the cracking surface

Mechanism of failure during Wedge Splitting Test (WST) was similar for plain concrete and concrete reinforced basalt fiber infused with boron as well. Crack had a non-uniform width and was strongly curved along sample depth and height (Figures 17Ac and 17Bc). The volume of crack in plain

concrete was equal 1063.5 mm^3 (0.39% of the entire sample) and was by about 28% higher than the volume of crack in concrete reinforced with basalt fiber infused with boron oxide equal 829.7 mm^3 (0.32% of the entire sample). Similar tendency was observed with reference to average and maximum crack width. Average and maximum crack width in plain concrete was $w_{c,av}$=0.38 mm and w_c=0.53 mm, which means that both values were by about 18% higher than average and maximum crack width in BBF concrete equal $w_{c,BBF,av}$=0.29 mm and $w_{c,BBF}$=0.46 mm, respectively. Basalt fibers infused with boron oxide used as a concrete dispersed reinforcement improved the ability of limiting maco-cracking width and macro-cracking volume.

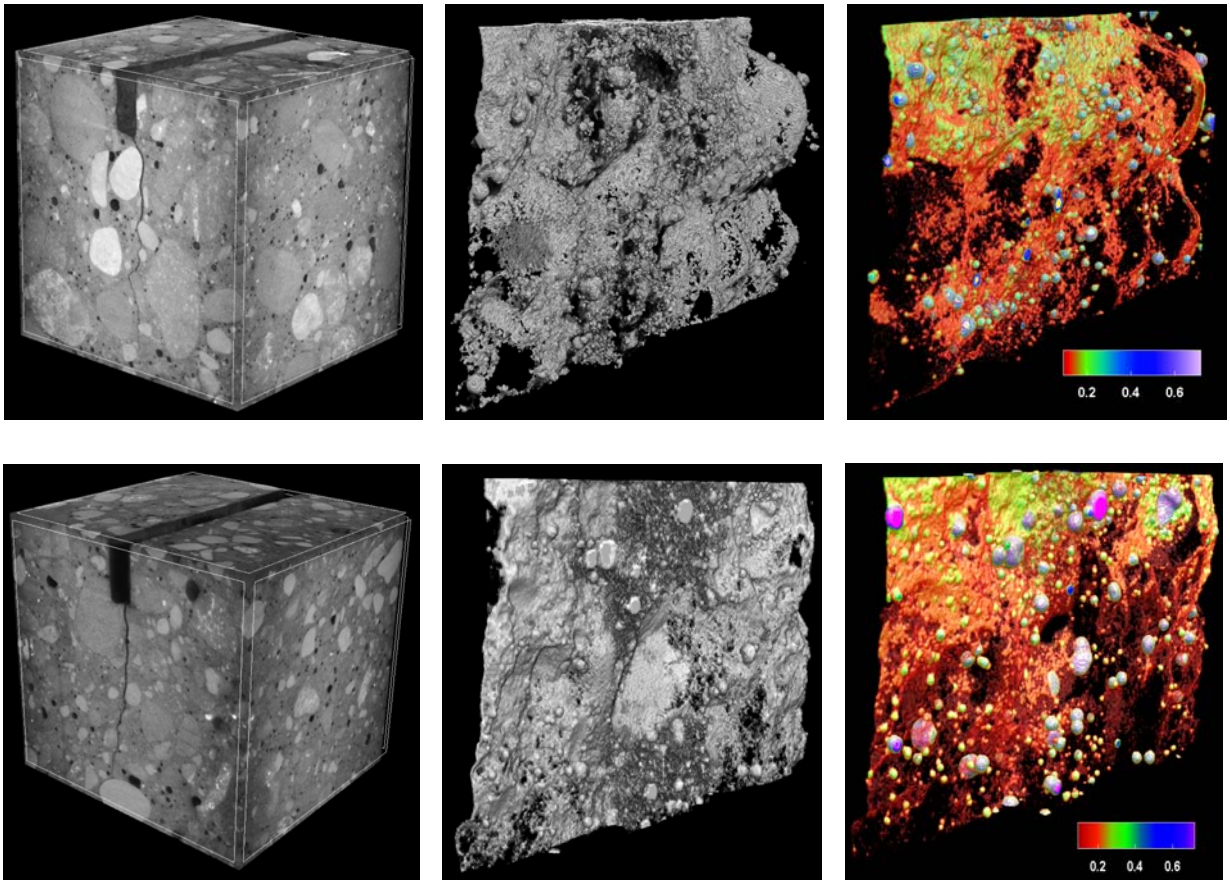

Figure 17: X-ray micro-CT images of cracked cubic specimens in Wedge Splitting Test (A) plain concrete and (B) BBF reinforced concrete where (a) 3D view of entire sample, (b) 3D view of crack and (c) 3D distribution of crack width

7. Conclusions

Investigations of the radiation shielding properties and mechanical properties of concrete reinforced with innovative basalt fibers infused with boron oxide (BBF) combined with the quantitative description of fracture phenomenon using Digital Image Correlation (DIC) and X-ray micro computed tomography (micro-CT) allow to draw the following conclusions:

(1) Addition of 5 kg/m^3 of BBF barely decreased concrete workability and fresh concrete density (by about 1.5%). Air pressure method test revealed that air content in fresh plain concrete was higher by about 20% than in fresh concrete reinforced with BBF. On the contrary, X-ray micro-CT experiments of hardened concrete revealed that, in fact, porosity of concrete reinforced with BBF was higher by about 30% than in plain concrete. Total porosity, determined by micro-CT, was smaller by about 10-30% than porosity received by air pressure

method test in case of plain and higher by about 15-40% in case of concrete reinforced with BBF. Obtained results clearly show that air pressure method may not be accurate.

(2) Experiments proved that concrete reinforcement in terms of basalt fibers infused with boron oxide may lead to the improvement of the neutron radiation shielding for fast neutron spectrum. Increase in neutron radiation shielding properties varies from 10% for layer thickness equal 50 cm to 25% for layer thickness equal 10 cm. Thus, it allows to be considered as a promising construction material for structures exposed to radioactive influence.

(3) Average compressive strength of plain concrete (f_c = 47.60 MPa) was higher by about 15% than of reinforced with BBF fibers ($f_{c,BBF}$ = 41.29 MPa). Average splitting strength of plain concrete (f_{ct} = 3.45 MPa) was higher by about 15% than of concrete reinforced with BBF fibers ($f_{ct,BBF}$ = 3.01 MPa). Average flexural strength of plain concrete ($f_{cf,}$ = 3.60 MPa) was higher by about 12.5% than of for concrete reinforced with BBF fibers ($f_{cf,BBF}$ = 3.20 MPa). However, the ratio of the tensile strength to the compression strength i.e. f_{ct} / f_c, $f_{cf,}$ / f_c and $f_{ct,BBF}$ / $f_{c,BBF}$, $f_{cf,BBF}$ / $f_{c,BBF}$ was similar for both mixes and equal 0.072 – 0.077. Mechanical properties may be affected by worse workability and higher porosity of concrete reinforced with BBF fibers.

(4) The average residual flexural tensile on strength (tested on beams 150×150×600 mm) of plain concrete were equal $f_{R,0.15}$ = 2.24 MPa, $f_{R,0.25}$ = 1.15 MPa and $f_{R,0.25}$ = 0.59 MPa and were higher by about 15% than the average residual tensile strength of concrete reinforced with BBF ($f_{R,0.15}$ = 2.06 MPa, $f_{R,0.25}$ = 0.99 MPa and $f_{R,0.35}$ = 0.52 MPa). On the contrary, during WST test, residual strength (tested on cubes 70×70×70 mm during wedge splitting test) in BBF reinforced concrete $F_{res,0.15}$=1.81 kN and $F_{res,0.25}$=0,72 kN were higher for about 20% - 90% than the residual strength in plain concrete $F_{res,0.15}$=1.48 kN and $F_{res,2.5}$=0.38 kN, respectively. WST test revealed that BBF concrete characterizes with greater ductility due to presence of fibers that have the ability of bridging micro-cracks.

(5) Final shrinkage strain for plain concrete was equal 1.65‰ whereas for concrete reinforced with BBF fibers was equal 1.52‰ (lower by about 10%). Increase of shrinkage shown similar tendency since the majority (80% of final shrinkage strain) of strain increase was observed within 14 days. Nevertheless, similar evolution of shrinkage strain curve and quite high final shrinkage strain leads to the conclusion that both type of concrete mixes require careful curing during early stages of hardening in order to minimize shrinkage cracking.

(6) Digital Image Correlation (DIC) technique revealed that maximum observed strains were equal about 0.07% and maximum horizontal displacements were equal about 0.11 mm for both mixes. The measured width of the fracture zone in plain concrete (w_{fz}=4.71 mm) was about 15% larger than in BBF concrete ($w_{fz,BBF}$=4.15 mm). It means that basalt fibers infused with boron oxide have the ability of limiting micro-cracking area. Moreover, the fracture zone length of the BBF concrete ($l_{fz,BBF}$=52.75 mm) was by about 10% greater than in plain concrete (l_{fz}=47.39 mm) which leads to the more ductile response in the softening regime. Macro-crack appeared, for both mixes, at about 85% of the peak load in the post-peak regime

(7) Compressive strength test combined with X-ray micro-CT scanning shown that mechanism of failure was similar for plain concrete and concrete reinforced basalt fibers infused with boron, however, wider cracks might have been observed in plain concrete. The vertical cracks that evolved through the entire height of the samples proved to be decisive. Nevertheless, diagonal cracks were noticed as well.

(8) Splitting strength test combined with X-ray micro-CT scanning shown that mechanism of failure was similar for plain concrete and concrete reinforced basalt fiber infused with boron, however, the surface of cracked area in concrete reinforced with basalts fiber infused with boron oxide ($A_{c,BFF}$=15766.58 mm^2) was about 9% higher than the surface of cracked area in plain concrete (A_c=14418.83 mm^2). It means that cracked area in BBF concrete is more curved so the evolution of the crack in BBF concrete is more sophisticated (crack is propagating between aggregate particles and micro fibers) than in plain concrete, thus, a more ductile response in a post-peak regime can be obtained.

(9) Wedge Splitting Test (WST) combined with X-ray micro-CT scanning proved that the volume of crack in plain concrete (1063.5 mm^3, 0.39% of the entire sample) was by about 28% higher than the volume of crack in concrete reinforced with basalt fibers infused with boron oxide (829.7 mm^3, 0.32% of the entire sample). Moreover, average and maximum crack width in plain concrete ($w_{c,av}$=0.38 mm and w_c=0.53 mm) were by about 18% higher than in BBF concrete ($w_{c,BBF,av}$=0.29 mm and $w_{c,BBF}$=0.46 mm). Basalt fibers infused with boron oxide used as a concrete dispersed reinforcement improved the ability of limiting macro-cracking width and macro-cracking volume.

(10) Dispersed reinforcement of concrete in terms of basalt fibers infused with boron oxide (BBF) improved the radiation protective properties of plain concrete without deterioration of its mechanical properties. In parallel, improvement of material durability due to limiting of micro-and macro-cracking was noticed.

7. Future perspectives

This paper presents preliminary investigations of concrete reinforced with 5 kg/m^3 of BBF, however, further studies concerning other dosages i.e. 1 kg/m^3, 10 kg/m^3, 15 kg/m^3 and 20 kg/m^3 as well as other i.e. 6% boron oxide B_2O_3 enrichment will be carried out.

Acknowledgements

Research work has been carried out as a part of the Project: "*Development of boron-induced basalt-fiber reinforced concrete for nuclear and radioactive waste management*" financed by the National Science Centre, Poland (2017/26/Z/ST8/01240).

References

[1] Bashter, I., El-Sayed Abdo, A. and Makarious, A. S. (1996) A comparative study of the attenuation of reactor thermal neutrons in different types of concrete. *Annals of Nuclear Energy*, **23(14)**, pp. 1189-1195.

[2] Kilincarslan, S., Akkurt, I. and Basyigit, C. (2006) The effect of barite rate on some physical and mechanical properties of concrete, *Materials Science and Engineering A*, **424(1-2)**, pp. 83-86.

[3] Chang-Min Lee, Yoon Hee Lee and Kun Jai Lee (2007) Cracking effect on gamma-ray shielding performance in concrete structure. *Progress in Nuclear Energy*, **49(4)**, pp. 303-312.

[4] Kharita, M., Takeyeddin, M., Alnassar, M. and Yousef, S. (2008) Development of special radiation shielding concretes using natural local materials and evaluation of their shielding characteristics, *Progress in Nuclear Energy*, **50(1)**, pp. 33-36.

[5] Kharita, M., Yousef, S. and Alnassar, M. (2010) The effect of the initial water to cement ratio on shielding properties of ordinary concrete. *Progress in Nuclear Energy*, **52(5)**, pp. 491-493.

[6] Kharita, M., Yousef, S. and Alnassar, M. (2011) Review on the addition compounds to radiation shielding concrete. *Progress in Nuclear Energy*, **53(2)**, pp. 207-211.
[7] Gencel, O., Bozkurt, A., Kam, E. and Korkut, T. (2011) Determining the gamma and neutron shielding characteristics of concretes containing different hematite proportions. *Annals of Nuclear Energy*, **38(12)**, pp. 2719-2723.
[8] Calzada, E., Grünauer, F., Schillinger, B. and Türck, H. (2011) Reusable shielding material for neutron- and gamma-radiation. *Nuclear Instruments and Methods in Physics Research Section A. Accelerators Spectrometers Detectors and Associated Equipment*, **651(1)**, pp. 77-80.
[9] Rezaeiochbelagh, D., Azimkhani, S. and Mosavinejad, H. (2011) Effect of gamma and lead as an additive material on the resistance and strength of concrete. *Nuclear Engineering and Design*, **241(6)**, pp. 2359-2363.
[10] Asano, Y. (2011) Application of heavy concretes to the shielding materials of synchrotron radiation beamlines. *Radiation Measurements,* **46(5)**, pp. 546-550.
[11] Mostofinejad, D. and Reisi, M. (2012) Mix design effective parameters on γ-ray attenuation coefficient and strength of normal and heavyweight concrete. *Construction and Building Materials*, **28(1)**, pp. 224-229.
[12] Kanasouh, W. A. (2012) Radiation distribution through serpentine concrete using local materials and its application as a reactor biological shield. *Annals of Nuclear Energy*, **47**, pp. 258-263.
[13] Bažant, Z. and Planas, J. (1997) Fracture and size effect in concrete and other quasi-brittle materials. *CRC Press LLC*, Boca Raton.
[14] Lilliu, G. and van Mier J. G. M. (2003) 3D lattice type fracture model for concrete. *Engineering Fracture Mechanics*, **70**, pp. 927-941.
[15] Skarżyński, Ł., Nitka, M. and Tejchman, J. (2015) Modelling of concrete fracture at aggregate level using FEM and DEM based on X-ray μCT images of internal structure. *Engineering Fracture Mechanics*, **147**, pp. 13-35.
[16] Gulik, V. I and Biland, A. B. (2012) The use of basalt, basalt fibers and modified graphite for nuclear waste repository. *Proceedings of Waste Management (WM2012) Conference, Phoenix, Arizona, USA*.
[17] Zorla, E., Ipbüker, C., Biland, A., Kiisk, M., Kovaljov, S., Tkaczyk, A. H. and Gulik, V. (2017) Radiation shielding properties of high performance concrete reinforced with basalt fibers infused with natural and enriched boron. *Nuclear Engineering and Design*, **313**, pp. 306-318.
[18] Ipbüker, C., Nulk, H., Gulik, V., Biland, A. and Tkaczyk, A. H. (2015) Radiation shielding properties of novel cement-based mixture for nuclear applications. *Nuclear Engineering and Design*, **284**, pp. 27-37.
[19] Corr, G., Accardi, M., Graham-Brady, L. and Shah, S. (2007) Digital image correlation analysis of interfacial debonding properties and fracture behavior in concrete. *Engineering Fracture Mechanics*, **74**, pp. 109-121.
[20] Wu, Z., Rong, H., Zheng, J. and Dong, W. (2011) An experimental investigation on the FPZ properties in concrete using digital image correlation technique. *Engineering Fracture Mechanics*, **78**, pp. 2978-2990.
[21] Alam, S. Y., Loukili, A. and Grondin, F. (2012) Monitoring size effect on crack opening in concrete by Digital Image Correlation. *European Journal of Environmental and Civil Engineering,* **16**, pp. 1-19.
[22] Bornert, M., Brémand, F., Doumalin, P., Dupré, J. C., Fazzini, M., Grédiac, M., Hild, F., Mistou, S., Molimard, J., Orteu, J. J., Robert, L., Surrel, Y., Vacher, P. and Wattrisse, B. (2009) Assessment of digital image correlation measurement errors: methodology and results. *Experimental Mechanics*, **49**, pp. 353–370.
[23] Helm, J. D., McNeill, S. R. and Sutton, M. A. (1996) Improved 3D image correlation for surface displacement measurement. *Optical Engineering*, **35**, pp. 1911–1920.

[24] Skarżyński, Ł. and Tejchman, J. (2010) Calculations of fracture process zones on meso-scale in notched concrete beams subjected to three-point bending. *European Journal of Mechanics A/Solids*, **29**, pp. 746-760.
[25] Skarżyński Ł. and Tejchman J., (2013) Experimental investigations of fracture process using DIC in plain and reinforced concrete beams under bending. *Strain*, **49(6)**, pp. 521-543.
[26] Skarżyński Ł, Kozicki J, Tejchman J. (2013) Application of DIC technique to concrete - study on objectivity of measured surface displacements. *Experimental Mechanics*, **53**, pp. 1545-1559.
[27] Mehdikhani, M., Aravand, M., Sabuncuoglu, B., Callens, M. G., Lomov, S. V. and Gorbatikh, L. (2016) Full-field strain measurements at the micro-scale in fiber-reinforced composites using digital image correlation. *Composite Structures*, **140**, pp. 192-201.
[28] Hamrat, M., Boulekbache, B., Chemrouk, M. and Amziane, S. (2016) Flexural cracking behaviour of normal strength, high strength and high strength fiber concrete beams using Digital Image Correlation technique. *Construction and Building Materials*, **106**, pp. 678-692.
[29] Ponikiewski, T., Katzer, J., Bugdol, M. and Rudzki, M. (2015) X-ray computed tomography harnessed to determine 3D spacing of steel fibers in self compacting (SCC) slabs. *Construction and Building Materials*, **74**, pp. 102-208.
[30] Ponikiewski, T., Gołaszewski, M., Rudzki, M. and Bugdol, M. (2015) Determination of steel fibres distribution in self-compacting concrete beams using X-ray computed tomography.. *Archives of Civil Engineering*, **2** pp. 558-568.
[31] Skarżyński Ł., Nitka M. and Tejchman J. (2015) Modelling of concrete fracture at aggregate level using FEM and DEM based on X-ray μCT images of internal structure, *Engineering Fracture Mechanics,* **147**, pp. 13-35.
[32] Balázs, G. L., Czobly, O., Lublóy, E., Kaplitány, K. and Barsi, A. (2017) Observation of steel fibers in concrete with Computed Tomography. *Construction and Building Materials,* **140**, pp. 534-541.
[33] Yua Q., Liub H., Yanga, T. and Liua, H. (2018) 3D numerical study on fracture process of concrete with different ITZ properties using X-ray computerized tomography. *International Journal of Solids and Structures,* **147**, pp. 204-222.
[34] Suchorzewski J., Tejchman J. and Nitka M. (2018) DEM simulations of fracture in concrete under uniaxial compression based on its real internal structure, *International Journal of Damage Mechanics*, **27(4)**, pp. 578-607.
[35] Skarżyński Ł. and Suchorzewski J. (2018) Mechanical and fracture properties of concrete reinforced with recycled and industrial steel fibers using Digital Image Correlation technique and X-ray micro computed tomography. *Construction and Building Materials,* **183**, pp. 283-299.
[36] Skarżynski Ł., Marzec I. and Tejchman J. (2018) Crack evolution in concrete compressive fatigue experiments based on X-ray micro-CT images. *International Journal of Fatigue,* **122**, pp. 256-272.
[37] Loeffler, C. M., Qiua Y., Martin B., Heard W., Williams B., Niea X. (2018) Detection and segmentation of mechanical damage in concrete with X-ray microtomography. *Materials Characterization,* **142**, pp. 515-522.
[38] Vicente, M. A., Ruiz, G., Gonzalez, D. C., Mínguez, J., Tarifa, M. and Zhang, X. X. (2018) CT-Scan study of crack patterns of fiber-reinforced concrete loaded monotonically and under low-cycle fatigue, *International Journal of Fatigue,* **114**, pp. 138-147.
[39] Vicente M.A., Mínguez J., and Gonzalez D.C. (2019) Computed tomography scanning of the internal microstructure, crack mechanisms and structural behaviour of fiber-reinforced concrete under static and cyclic bending tests, *International Journal of Fatigue,* **121**, pp. 1-19.
[40] Skarżyński Ł. and Tejchman J. (2019) Experimental investigations of damage evolution in concrete during bending by continuous micro-CT scanning. *Materials Characterization,* **154**, pp. 40-52.

[41] Ríos, J. D., Leive, C., Ariza, M. P., Seitl, S. and Cifuentes, H. (2019) Analysis of the tensile fracture properties of ultra-heigh-strength fiber-reinforced concrete with different types of steel fibers by X-ray tomography. Materials and Design, **165**, pp. 1-14.
[42] EN 12390-3:2009 Testing hardened concrete – Part 3: Compressive strength of test specimens.
[43] EN 12390-6:2011 Testing hardened concrete – Part 6: Tensile splitting strength of test specimens.
[44] EN 14651:2005+A1:2007 Test method for metallic fiber concrete. Measuring the flexural tensile strength (limit of proportionality (LOP), residual).
[45] EN 12390-2:2009 Testing hardened concrete – Part 2: Making and curing specimens for strength tests.
[46] Instrukcja ITB 194/98 Badanie cech mechanicznych betonu na próbkach wykonanych w formach (in polish).
[47] Lecompte, D., Smits, A., Bossuyt, S., Sol, H., Vantomme, J., van Hemelrijck, D., Habraken, A. M. (2006) Quality assessment of speckle patterns for digital image correlation. *Optical and Lasers in Engineering*, **44**, pp. 1132-1145.
[48] Pan, B., Xie, H., Wang, Z., Qian, K. and Wang, Z. (2008) Study on subset size selection in digital image correlation for spackle patterns. *Optics Express*, **16**, pp. 7037-7048
[49] Ponikiewski, T., Katzer, J., Bugdol, M. and Rudzki, M. (2014) Determination of 3D porosity in steel fibre reinforced SCC beams using X-ray computed tomography. *Construction and Building Materials,* **68**, pp. 333–340.
[50] Nguyen, T., Bui, H., Tuan, D., Ngo, T. and Nguyen, G. (2017) Experimental and numerical investigation of influence of air-voids on the compressive behaviour of foamed concrete. *Materials & Design,* **130**, pp. 103–119.
[51] Bayasi, M. Z. and Soroushian, P. (1992) Effect of steel fiber reinforcement on fresh mix properties of concrete. *ACI Materials Journal,* **89**, pp. 369-374.
[52] Page, J., Khadraoui, F., Boutouil, M. and Gomina, M. (2017) Multi-physical properties of a structural concrete incorporating short flax fibers. *Construction and Building Materials,* **140**, pp. 344-353.
[53] Guerini, V., Conforti, A., Plizzari, G. A. and Kawashima, S. (2018) Influence of steel and macro-synthetic fibers on concrete properties. *Fibers,* **6(47)**, doi.org/10.3390/fib6030047
[54] Balaguru, P., Ramakrishnan, V. (1988) Properties of fiber reinforced concrete: workability, behaviour under long-term loading and air-void characteristics. *ACI Materials Journal,* **85**, pp. 189-196.
[55] Skarżyński, Ł. and Tejchman, J. (2013) Modeling the effect of material composition on the tensile properties of concrete. Understanding the tensile properties of concrete. *Woodhead Publishing Series in Civil and Structural Engineering*, pp. 52-97.
[56] Skarżyński, Ł. and Tejchman, J. (2019) Experimental investigations of damage evolution in concrete during bending by continuous micro-CT scanning. *Materials Characterization*, **154**, pp. 40-52.